J. Plasma Physics (2001), *vol.* 66, *part* 5, *pp.* 349–362.
DOI: 10.1017/S0022377801001489 Printed in the United Kingdom

Propagation of surface waves in two-plasma systems bounded by a metallic enclosure

LUC STAFFORD,[1] JOËLLE MARGOT[1]
and TUDOR W. JOHNSTON[2]

[1]Département de Physique, Université de Montréal, Montréal, Québec, Canada
[2]INRS–Énergie et Matériaux, Varennes, Québec, Canada

(Received 22 June 2001)

Abstract. This paper examines the possibility of propagating surface waves in cylindrical plasma–plasma structures enclosed by metal walls and submitted or not to a static magnetic field. We consider the situation in which the inner plasma layer is overdense while the other is underdense. It is shown that outside the electron cyclotron resonance (ECR) conditions, the outer plasma layer plays a role similar to that of an ordinary dielectric layer, just modifying the wavenumber without drastically changing the general characteristics of the wave. At ECR, a major change in the wavenumber and attenuation coefficient is observed, a cutoff occurring on the left side of ECR and a resonance on the right side, provided the outer plasma density is large enough. It is further found that in conditions where the outer plasma layer thickness is very small, wave propagation still occurs, whatever the density value in this region. This suggests that surface wave propagation is possible in plasma–sheath–metal structures.

1. Introduction

Over the last three decades, the characteristics of electromagnetic surface waves have been widely investigated under a variety of conditions, essentially because of their interest for sustaining plasmas under wide experimental conditions and configurations. Reviews reporting the generation of plasmas with electromagnetic surface waves can be found in Zhelyazkov and Atanassov (1994) and Moisan et al. (1999). Initially designated as space-charge waves, the existence of surface waves was first predicted theoretically by Trivelpiece and Gould (1959) as electromagnetic waves guided by the interface between a plasma and a dielectric layer. Surface waves were subsequently shown to be an efficient means of sustaining reproducible and quiescent plasmas of interest for many applications, in particular materials processing. The concept of surface wave can be generalized to the case of plasmas submitted to magnetic field (Pasquiers et al. 1989; Margot and Moisan 1991), in which case the surface wave is generally known as the Trivelpiece–Gould mode (Trivelpiece 1967).

In the absence or in the presence of a magnetic field, the plasmas sustained by surface waves are characterized by their exceptional tunability in terms of plasma parameters (pressure, vessel dimensions, wave frequency, etc.), which is well adapted to a parametric investigation of the influence of these parameters on the plasma

characteristics. In this respect, surface-wave plasmas are thus unique among the class of plasmas generated by electromagnetic energy, and they have been used as a means of characterizing high-frequency plasmas in general (Ferreira and Moisan 1988).

The most common configuration employed (and the oldest) is cylindrical geometry, but recent work performed by Japanese groups, in particular at Nagoya University, has shown the possibility of using planar geometries (Sugai et al. 1998). Industrial high-density reactors based on surface waves in planar configuration are now commercialized and used, in particular, for nanometric etching of thin films.

In the most usual situations, the surface wave is excited at the gap of a wave launcher (surfatron, Ro-box, etc.) especially designed for optimizing the conversion of the electromagnetic energy into a surface wave (Moisan and Zakrzewski 1991). This wave launcher is located at the outside of a dielectric vessel transparent to high frequencies, i.e. exhibiting a low loss tangent (e.g. fused silica). In the context of applications of surface-wave plasmas, it is, however, highly desirable to minimize dielectric materials, which are expensive, fragile, and thus difficult to handle, and to replace them by metal, such as stainless-steel. Another useful property of metals is that, provided they are adequately chosen, they are more resistant to chemical attack by reactive gases. For example, stainless steel is usually considered as relatively inert with respect to chlorinated and fluorinated gases. Finally, a metallic vessel is likely to screen the environment more efficiently from radiation problems.

Interest in surface-wave plasmas was until recently limited in the user community because it was believed that a metallic vessel could not support surface-wave propagation. This belief is based on the fact that it was previously shown that surface waves are unable to propagate in plasma–metal structures, simply because it is impossible to satisfy the boundary conditions. However, recent experimental work by Morita et al. (1998) has shown that surface waves are suspected to be responsible for the generation of an unmagnetized metal-bound plasma discharge. This is additionally supported by PIC–Monte Carlo calculations (Coopersberg and Birdsall 1998). The reason why propagation is possible is related to the fact that the plasma is actually never in direct contact with the metal wall but is separated from it by at least a sheath, which acts as a thin dielectric layer. In other situations, the plasma is formed by several plasma layers of different densities (hence different permittivities), so that the actual configuration is more complicated that a simple plasma–metal structure.

In the present paper, we address this question by examining the possibility of propagating electromagnetic surface waves in cylindrical plasma–plasma–metal structures where the inner plasma is overdense and the outer one underdense. Note that when the outer plasma density becomes very low so that its permittivity approaches unity, it can be considered as free space. In Sec. 2, we describe the configuration under investigation and we solve the Maxwell equations with the appropriate boundary conditions. The numerical results are further presented and discussed in Sec. 3. Finally, we conclude in Sec. 4.

2. Resolution of the Maxwell equations for a cylindrical plasma–plasma–metal system

The configuration under investigation is shown in Fig. 1 and corresponds to an experimental setup designed for the etching of thin films. It has been described in

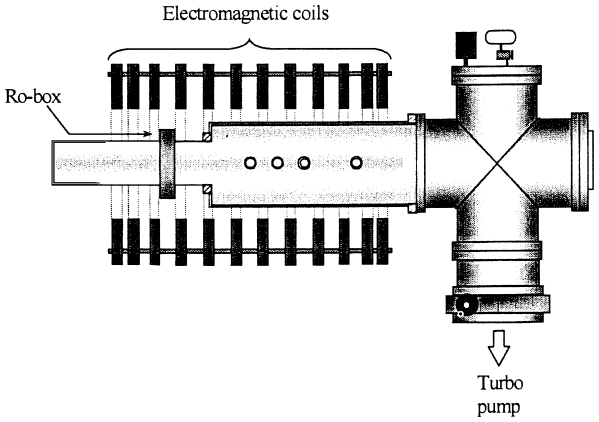

Figure 1. Schematic drawing of the experimental arrangement.

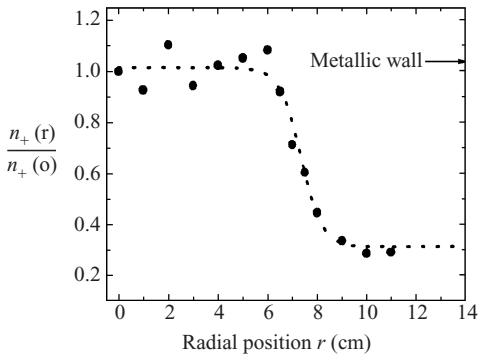

Figure 2. Plasma density profile in the stainless-steel chamber of the reactor shown in Fig. 1 for a magnetic field intensity of 300 G at a gas pressure of 1 mTorr and a wave frequency of 190 MHz.

detail elsewhere (see e.g. St-Onge et al. 1998; Delprat et al. 1999). It consists of two abutting cylinders, one made of fused silica (14.6 cm inner diameter) and the other one of stainless-steel (28 cm inner diameter). A 190 MHz surface wave is excited at the launching gap of a Ro-box located around the dielectric vessel. The plasma is created in the dielectric vessel and extends into the stainless-steel chamber. The plasma can be confined by a magnetic field set of 12 coils connected in series and that can be varied continuously from 0 to over 1 kG. The question addressed in this paper concerns wave propagation in the stainless-steel chamber, in the presence or not of the magnetic field.

Measurements of plasma density distribution in this reactor show that in the absence of a magnetic field, the plasma tends to fill the whole stainless-steel reactor in both the radial and the axial directions, provided the gas pressure is low enough (typically below 10 mTorr). When a magnetic field of sufficient strength is applied, the plasma tends to contract to a radius corresponding to that of the dielectric tube, as illustrated in Fig. 2. In this case, it is thus reasonable to model the plasma as consisting in two layers of radius a and b with different permittivities.

For simplicity, we consider here that the density is constant in each plasma layer. As a consequence, the configuration will be assumed to be that of Fig. 3, consisting

https://doi.org/10.1017/S0022377801001489 Published online by Cambridge University Press

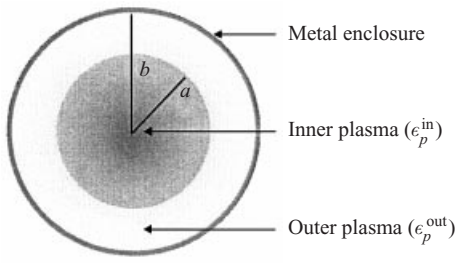

Figure 3. Configuration considered for calculations.

of two concentric cylindrical spatially homogeneous plasma columns of infinite axial extent surrounded by a metal enclosure. We denote the inner plasma permittivity by $\boldsymbol{\epsilon}_p^{\text{in}}$ and the outer one by $\boldsymbol{\epsilon}_p^{\text{out}}$.

Both plasma layers are submitted to an electromagnetic field of angular frequency ω large enough for ions to be immobile in the wave electric field. In the presence of a static magnetic field in the z direction of a cylindrical coordinate system, each plasma layer can be described in the cold-plasma approximation as a dielectric of tensorial relative permittivity $\boldsymbol{\epsilon}_p$ given by

$$\boldsymbol{\epsilon}_p = \begin{pmatrix} \epsilon_1 & -\epsilon_2 & 0 \\ \epsilon_2 & \epsilon_1 & 0 \\ 0 & 0 & \epsilon_3 \end{pmatrix}, \tag{2.1}$$

where ϵ_1, ϵ_2 and ϵ_3 are defined as

$$\epsilon_1 = 1 - \xi^2 \frac{1 - i\delta}{(1 - i\delta)^2 - \tau^2}, \tag{2.2a}$$

$$\epsilon_2 = \frac{i\tau\xi^2}{(1 - i\delta)^2 - \tau^2}, \tag{2.2b}$$

$$\epsilon_3 = 1 - \frac{\xi^2}{1 - i\delta}, \tag{2.2c}$$

with $i = \sqrt{-1}$, where $\xi^2 = \omega_p^2/\omega^2$, $\delta = \nu/\omega$ and $\tau = \omega_c/\omega$. Here ω_p, ω_c, and ν are respectively the angular plasma frequency, the angular electron cyclotron frequency, and the effective electron–neutral collision frequency for momentum transfer (Shkarofski et al. 1966).

Given $\boldsymbol{\epsilon}_p$, we search for solutions of the form $\exp(i\omega t - \gamma z)$, where $\gamma = \alpha + i\beta$, α and β being the axial components of the attenuation coefficient and wavenumber. The Maxwell equations lead to the following two relations coupling the wave electric and magnetic fields $\mathbf{E}$ and $\mathbf{H}$ (Allis et al. 1963):

$$\nabla_\perp^2 E_z + q_1 E_z = q_2 H_z, \tag{2.3}$$

$$\nabla_\perp^2 H_z + q_3 H_z = q_4 E_z. \tag{2.4}$$

Here $\nabla_\perp^2$ is the Laplacian in the transverse direction, and the constants q_1, q_2, q_3 and q_4 are defined as

$$q_1 = (\gamma^2 + \beta_0^2 \epsilon_1)\frac{\epsilon_3}{\epsilon_1}, \tag{2.5}$$

$$q_2 = i\omega\mu_0\gamma\frac{\epsilon_2}{\epsilon_1}, \tag{2.6}$$

https://doi.org/10.1017/S0022377801001489 Published online by Cambridge University Press

$$q_3 = (\gamma^2 + \beta_0^2\epsilon_1)\frac{\epsilon_1^2 + \epsilon_2^2}{\epsilon_1}, \tag{2.7}$$

$$q_4 = -i\omega\epsilon_0\gamma\frac{\epsilon_2\epsilon_3}{\epsilon_1}. \tag{2.8}$$

Here $\beta_0 = 2\pi/\lambda_0 = \omega/c$ denotes the free-space wavenumber, where c is the speed of light in free space. More details about the calculations required to obtain a solution of (2.3) and (2.4) can be found, for example, in Margot and Moisan (1991). Briefly, (2.3) and (2.4) can be rearranged to yield

$$\nabla_\perp^4 E_z + (q_1 + q_3)\nabla_\perp^2 E_z + (q_1 q_3 - q_2 q_4)E_z = 0, \tag{2.9}$$

$$\nabla_\perp^4 H_z + (q_1 + q_3)\nabla_\perp^2 E_z + (q_1 q_3 - q_2 q_4)H_z = 0. \tag{2.10}$$

Defining

$$(q_1 + q_3) = p_1^2 + p_2^2 \tag{2.11}$$

and

$$(q_1 q_3 - q_2 q_4) = p_1^2 p_2^2, \tag{2.12}$$

(2.9) becomes

$$(\nabla_\perp^2 + p_1^2)(\nabla_\perp^2 + p_2^2)E_z = 0, \tag{2.13}$$

which yields two solutions:

$$(\nabla_\perp^2 + p_1^2)E_{z1} = 0, \tag{2.14}$$

$$(\nabla_\perp^2 + p_2^2)E_{z2} = 0. \tag{2.15}$$

In each medium, the axial component of the electric field generally consists of the superposition of two elementary components: E_{z1} and E_{z2} (Margot and Moisan 1991). In a cylindrical coordinate system, (2.14) and (2.15) can be solved by the method of separation of variables, leading to the solution

$$E_z = [B_1\mathscr{F}_m(p_1 r) + B_2\mathscr{F}_m(p_2 r)]\exp(im\phi - \gamma z + i\omega t), \tag{2.16}$$

where B_1 and B_2 are constants, the relative weight of which is determined by the boundary conditions, and where m is an integer (the azimuthal wavenumber); $\mathscr{F}_m$ is the superposition of two Bessel functions. For convenience, it is useful to choose the Bessel function J_m and the Hankel function $H_m^{(1)}$ because of their behavior at $r = 0$ and $r \to \infty$, respectively. It can be readily verified that (as one might expect) p_1 and p_2 are in fact the two distinct wavenumber components perpendicular to the magnetic field given by solving the cold-plasma dispersion relation for the current value of the plasma parameters, of ω and of the single wavenumber component parallel to the magnetic field, γ. The expression for the magnetic field H_z is obtained by inserting (2.16) into (2.3):

$$H_z = [B_1 h_1\mathscr{F}_m(p_1 r) + B_2 h_2\mathscr{F}_m(p_2 r)]\exp(im\phi - \gamma z + i\omega t), \tag{2.17}$$

where $h_i = (q_1 - p_i^2)/q_2$. The other electromagnetic field components can be deduced

https://doi.org/10.1017/S0022377801001489 Published online by Cambridge University Press

in a straightforward manner from the transformation matrix

$$\begin{pmatrix} E_r \\ E_\phi \\ H_r \\ H_\phi \end{pmatrix} = \begin{pmatrix} A_{11} & -A_{12} & A_{31} & A_{32} \\ A_{12} & A_{11} & -A_{32} & A_{31} \\ A_{13} & -A_{14} & -A_{11} & A_{12} \\ A_{14} & A_{13} & -A_{12} & -A_{11} \end{pmatrix} \begin{pmatrix} -\dfrac{im}{r}E_z \\ \nabla_r E_z \\ \dfrac{im}{r}H_z \\ -\nabla_r H_z \end{pmatrix}, \tag{2.18}$$

where the elements A_{ij} are defined as

$$A_{11} = \frac{\beta_0^2 \epsilon_2 \gamma}{D}, \tag{2.19}$$

$$A_{12} = \frac{\gamma(\beta_0^2 \epsilon_1 + \gamma^2)}{D}, \tag{2.20}$$

$$A_{13} = -\frac{i\omega\epsilon_0[\beta_0^2(\epsilon_1^2 + \epsilon_2^2) + \epsilon_1\gamma^2]}{D}, \tag{2.21}$$

$$A_{14} = -\frac{\gamma^2 i\omega\epsilon_0\epsilon_2}{D}, \tag{2.22}$$

$$A_{31} = -\frac{i\omega\mu_0(\beta_0^2\epsilon_1 + \gamma^2)}{D}, \tag{2.23}$$

$$A_{32} = -\frac{i\omega\mu_0\beta_0^2\epsilon_2}{D}, \tag{2.24}$$

with $D = (\gamma^2 + \beta_0^2\epsilon_1)^2 + \beta_0^4\epsilon_2^2$. For the considered plasma–plasma configuration and for the case of the azimuthally symmetric mode $m = 0$, expressions for the electromagnetic field components in the three directions z, r and ϕ can be deduced from (2.16)–(2.18):

$$\begin{aligned} E_z^k = {} & B_1^k J_0(p_1^k r) + B_2^k J_0(p_2^k r) \\ & + B_3^k H_0^{(1)}(p_1^k r) + B_4^k H_0^{(1)}(p_2^k r), \end{aligned} \tag{2.25}$$

$$\begin{aligned} H_z^k = {} & B_1^k l_1^k J_0(p_1^k r) + B_2^k l_2^k J_0(p_2^k r) \\ & + B_3^k l_1^k H_0^{(1)}(p_1^k r) + B_4^k l_2^k H_0^{(1)}(p_2^k r), \end{aligned} \tag{2.26}$$

$$\begin{aligned} E_\phi^k = {} & [B_1^k J_1(p_1^k r) + B_3^k H_1^{(1)}(p_1^k r)](-A_{11}^k p_1^k + A_{31}^k l_1^k p_1^k) \\ & + [B_2^k J_1(p_2^k r) + B_4^k H_1^{(1)}(p_2^k r)](-A_{11}^k p_2^k + A_{31}^k l_2^k p_2^k), \end{aligned} \tag{2.27}$$

$$\begin{aligned} H_\phi^k = {} & [B_1^k J_1(p_1^k r) + B_3^k H_1^{(1)}(p_1^k r)](-A_{13}^k p_1^k - A_{11}^k l_1^k p_1^k) \\ & + [B_2^k J_1(p_2^k r) + B_4^k H_1^{(1)}(p_2^k r)](-A_{13}^k p_2^k - A_{11}^k l_2^k p_2^k), \end{aligned} \tag{2.28}$$

$$\begin{aligned} E_r^k = {} & [B_1^k J_1(p_1^k r) + B_3^k H_1^{(1)}(p_1^k r)](A_{12}^k p_1^k + A_{32}^k l_1^k p_1^k) \\ & + [B_2^k J_1(p_2^k r) + B_4^k H_1^{(1)}(p_2^k r)](A_{12}^k p_2^k + A_{32}^k l_2^k p_2^k), \end{aligned} \tag{2.29}$$

$$\begin{aligned} H_r^k = {} & [B_1^k J_1(p_1^k r) + B_3^k H_1^{(1)}(p_1^k r)](A_{14}^k p_1^k + A_{12}^k l_1^k p_1^k) \\ & + [B_2^k J_1(p_2^k r) + B_4^k H_1^{(1)}(p_2^k r)](A_{14}^k p_2^k + A_{12}^k l_2^k p_2^k), \end{aligned} \tag{2.30}$$

where k = in, out refers to either the inner or the outer plasma. The application of boundary conditions implies that B_3^{in} and B_4^{in} are zero, since the solution must

https://doi.org/10.1017/S0022377801001489 Published online by Cambridge University Press

remain finite at $r = 0$. The tangential components of the electric field must also be zero at the metal enclosure ($r = b$), since $\hat{\boldsymbol{n}} \times \mathbf{E} = 0$ at the surface of a conductor. The system thus reduces to only four constants with B_1^{out} and B_2^{out}, which can be written in terms of B_3^{out} and B_4^{out} as

$$B_2^{\text{out}} = D_1 B_3^{\text{out}} + D_2 B_4^{\text{out}}, \tag{2.31}$$

$$B_2^{\text{out}} = D_3 B_3^{\text{out}} + D_4 B_4^{\text{out}}, \tag{2.32}$$

where the constants D_n are defined as

$$D_1 = \frac{\dfrac{H_0^{(1)}(p_1^{\text{out}}b)}{J_0(p_1^{\text{out}}b)} - \dfrac{H_1^{(1)}(p_1^{\text{out}}b)}{J_1(p_1^{\text{out}}b)}}{\dfrac{M_2^{\text{out}}J_1(p_2^{\text{out}}b)}{M_1^{\text{out}}J_1(p_1^{\text{out}}b)} - \dfrac{J_0(p_2^{\text{out}}b)}{J_0(p_1^{\text{out}}b)}}, \tag{2.33}$$

$$D_2 = \frac{\dfrac{H_0^{(1)}(p_2^{\text{out}}b)}{J_0(p_1^{\text{out}}b)} - \dfrac{M_2^{\text{out}}H_1^{(1)}(p_2^{\text{out}}b)}{M_1^{\text{out}}J_1(p_1^{\text{out}}b)}}{\dfrac{M_2^{\text{out}}J_1(p_2^{\text{out}}b)}{M_1^{\text{out}}J_1(p_1^{\text{out}}b)} - \dfrac{J_0(p_2^{\text{out}}b)}{J_0(p_1^{\text{out}}b)}}, \tag{2.34}$$

$$D_3 = -\frac{J_0(p_2^{\text{out}}b)}{J_0(p_1^{\text{out}}b)} D_1 - \frac{H_0^{(1)}(p_1^{\text{out}}b)}{J_0(p_1^{\text{out}}b)}, \tag{2.35}$$

$$D_4 = -\frac{J_0(p_2^{\text{out}}b)}{J_0(p_1^{\text{out}}b)} D_2 - \frac{H_0^{(1)}(p_2^{\text{out}}b)}{J_0(p_1^{\text{out}}b)}. \tag{2.36}$$

The constants M_j^k are given by

$$M_j^k = -A_{11}^k p_j^k + A_{31}^k l_j^k p_j^k. \tag{2.37}$$

The application of boundary conditions at the inner–outer plasma interface ($r = a$) implies that the tangential components of the electric and magnetic fields are continuous, i.e.

$$\begin{pmatrix} (E_z^{\text{in}} - E_z^{\text{out}})_{r=a} \\ (H_z^{\text{in}} - H_z^{\text{out}})_{r=a} \\ (E_\phi^{\text{in}} - E_\phi^{\text{out}})_{r=a} \\ (H_\phi^{\text{in}} - H_\phi^{\text{out}})_{r=a} \end{pmatrix} = \mathbf{T} \begin{pmatrix} B_1^{\text{in}} \\ B_2^{\text{in}} \\ B_3^{\text{out}} \\ B_4^{\text{out}} \end{pmatrix}, \tag{2.38}$$

where the elements T_{ij} of the matrix $\mathbf{T}$ are given by

$$T_{11} = J_0(p_1^{\text{in}}a), \tag{2.39}$$

$$T_{12} = J_0(p_2^{\text{in}}a), \tag{2.40}$$

$$T_{13} = -[D_1 J_0(p_1^{\text{out}}a) + D_3 J_0(p_1^{\text{out}}a) + H_0^{(1)}(p_1^{\text{out}}a)], \tag{2.41}$$

$$T_{14} = -[D_2 J_0(p_1^{\text{out}}a) + D_4 J_0(p_1^{\text{out}}a) + H_0^{(1)}(p_2^{\text{out}}a)], \tag{2.42}$$

$$T_{21} = l_1^{\text{in}} J_0(p_1^{\text{in}}a), \tag{2.43}$$

$$T_{22} = l_2^{\text{in}} J_0(p_2^{\text{in}}a), \tag{2.44}$$

$$T_{23} = -[l_1^{\text{out}} D_1 J_0(p_1^{\text{out}}a) + l_2^{\text{out}} D_3 J_0(p_1^{\text{out}}a) + l_1^{\text{out}} H_0^{(1)}(p_1^{\text{out}}a)], \tag{2.45}$$

https://doi.org/10.1017/S0022377801001489 Published online by Cambridge University Press

$$T_{24} = -[l_1^{\text{out}} D_2 J_0(p_1^{\text{out}} a) + l_2^{\text{out}} D_4 J_0(p_1^{\text{out}} a) + l_2^{\text{out}} H_0^{(1)}(p_2^{\text{out}} a)], \tag{2.46}$$

$$T_{31} = M_1^{\text{in}} J_1(p_1^{\text{in}} a), \tag{2.47}$$

$$T_{32} = M_2^{\text{in}} J_1(p_2^{\text{in}} a), \tag{2.48}$$

$$T_{33} = -[M_1^{\text{out}} D_1 J_1(p_1^{\text{out}} a) + M_2^{\text{out}} D_3 J_1(p_1^{\text{out}} a) + M_1^{\text{out}} H_1^{(1)}(p_1^{\text{out}} a)], \tag{2.49}$$

$$T_{34} = -[M_1^{\text{out}} D_2 J_1(p_1^{\text{out}} a) + M_2^{\text{out}} D_4 J_1(p_1^{\text{out}} a) + M_2^{\text{out}} H_1^{(1)}(p_2^{\text{out}} a)], \tag{2.50}$$

$$T_{41} = Q_1^{\text{in}} J_1(p_1^{\text{in}} a), \tag{2.51}$$

$$T_{42} = Q_2^{\text{in}} J_1(p_2^{\text{in}} a), \tag{2.52}$$

$$T_{43} = -[Q_1^{\text{out}} D_1 J_1(p_1^{\text{out}} a) + Q_2^{\text{out}} D_3 J_1(p_1^{\text{out}} a) + Q_1^{\text{out}} H_1^{(1)}(p_1^{\text{out}} a)], \tag{2.53}$$

$$T_{44} = -[Q_1^{\text{out}} D_2 J_1(p_1^{\text{out}} a) + Q_2^{\text{out}} D_4 J_1(p_1^{\text{out}} a) + Q_2^{\text{out}} H_1^{(1)}(p_2^{\text{out}} a)], \tag{2.54}$$

the constants Q_j^k being defined as

$$Q_j^k = -A_{13}^k p_j^k - A_{11}^k l_j^k p_j^k. \tag{2.55}$$

In order to obtain a non-trivial solution for the electromagnetic field, the determinant of the matrix $\mathbf{T}$ must be zero. For given conditions, this is verified only for a discrete number of values of γ.

We have solved this determinental equation using a Müler method with deflation. Since the calculation consist in solving a transcendental equation in the complex plane, there are an infinite number of discrete roots. To ensure that only the solutions corresponding to a surface wave are found (note that below the electron cyclotron resonance (ECR), there is only one surface-wave solution), we start from known surface wave solutions obtained in standard situations already studied.

It is customary when describing wave propagation in plasmas to present dispersion curves as Brillouin diagrams with ω/ω_p as vertical axis. In such diagrams, ω_p is usually constant while ω varies. In the case of surface waves, however, it is usual to present curves in which ω is kept constant while ω_p varies, thus yielding a phase diagram rather than a dispersion diagram. In the following, we will present results obtained at a frequency of 190 MHz for varying inner and outer plasma densities.

3. Numerical results

3.1. Influence of plasma densities and magnetic field intensity on the wave characteristics

Figures 4(a) and 4(b) show the phase and the attenuation coefficient as functions of $\omega/\omega_p^{\text{in}}$ for different values of the outer plasma density in an unmagnetized weakly collisional plasma ($\nu/\omega = 10^{-3}$). Note that the case where $\omega/\omega_p^{\text{out}} = 100$ approaches the situation of a plasma surrounded by free space and a metal enclosure. It can be seen from Fig. 4(a) that for decreasing $\omega/\omega_p^{\text{out}}$, the wavenumber β decreases. In addition, its relative variation with $\omega/\omega_p^{\text{in}}$ is less important, i.e. the structure becomes less and less dispersive. One also notices that in the lower part of the phase diagram, i.e. for small $\omega/\omega_p^{\text{in}}$ values, and for small $\omega/\omega_p^{\text{out}}$, the wave becomes fast ($\beta < \beta_0$ where $\beta_0 = 3.98\,\text{m}^{-1}$ for $f = 190\,\text{MHz}$). As far as the attenuation coefficient is concerned, Fig. 4(b) shows that for a given outer plasma density, α increases with $\omega/\omega_p^{\text{in}}$, as is always observed for a forward $m = 0$ surface wave. Finally, for a constant inner plasma density, it can be seen that α increases with the

https://doi.org/10.1017/S0022377801001489 Published online by Cambridge University Press

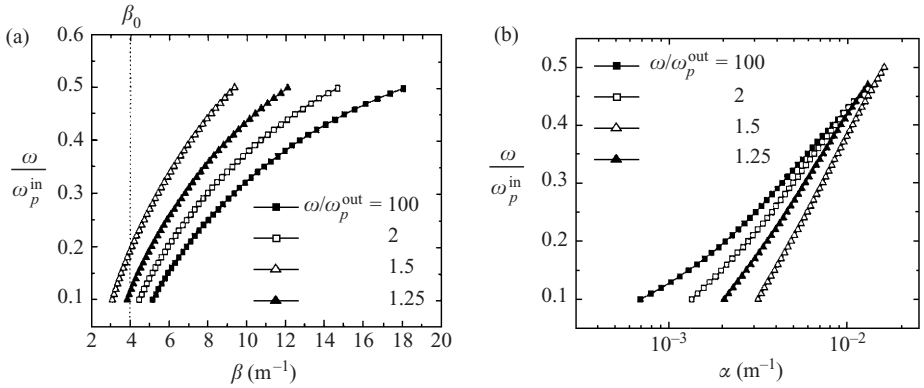

Figure 4. Phase and attenuation diagrams for different outer plasma densities in a weakly collisional ($\nu/\omega = 10^{-3}$) and unmagnetized plasma.

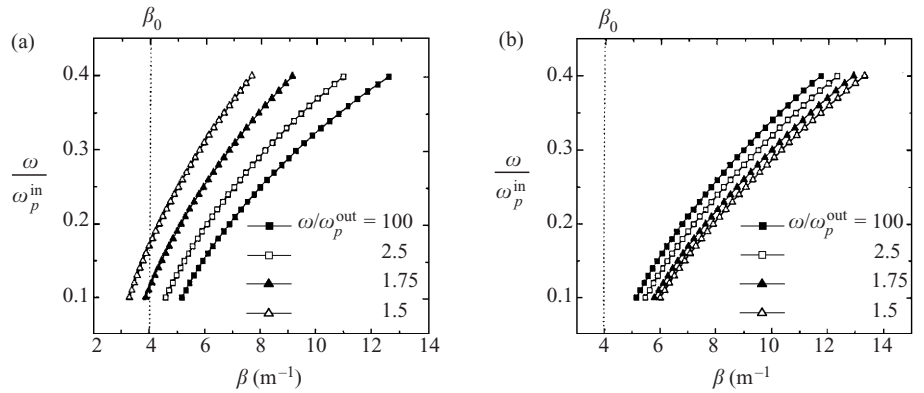

Figure 5. Phase diagrams for different outer plasma densities and for two values of the magnetic field intensity: (a) $\omega_c/\omega = 0.5$; (b) $\omega_c/\omega = 1.5$.

outer plasma density. We expect that as the outer plasma tends toward its critical value ($\omega/\omega_p^{out} = 1$), $\beta \to 0$ (this condition corresponds to a cutoff) and $\alpha \to \infty$.

Figures 5(a) and 5(b) show the phase diagrams when a magnetic field is applied to the system. Figure 5(a) corresponds to a value of $\omega_c/\omega = 0.5$, i.e. below the ECR, while Fig. 5(b) was obtained for $\omega_c/\omega = 1.5$. As can be seen, below the ECR, the axial wavenumber decreases with ω/ω_p^{out}. In contrast, above the ECR, β increases with the outer plasma density. These results clearly show that a change in the wave behavior occurs on both sides of ECR. This behavior differs drastically from that observed for the plasma–air or plasma–dielectric–air cases (Margot and Moisan 1997). In addition, the influence of the outer plasma density on the phase diagram is less important above the ECR.

The results obtained in Figs 5(a) and 5(b) can be summarized by showing β as a function of ω_c/ω for a given inner plasma density and for different ω/ω_p^{out}. This is illustrated in Fig. 6, which confirms the fact that a drastic change in the wave characteristics occurs at $\omega_c/\omega = 1$ when the outer plasma density increases. However, when the outer plasma density is decreasing to 0 (i.e $\omega/\omega_p^{out} \to \infty$), the amplitude of this change is less and less important, until no more discontinuity is observed for $\omega/\omega_p^{out} = 1000$, presumably because the corresponding plasma density is so low

https://doi.org/10.1017/S0022377801001489 Published online by Cambridge University Press

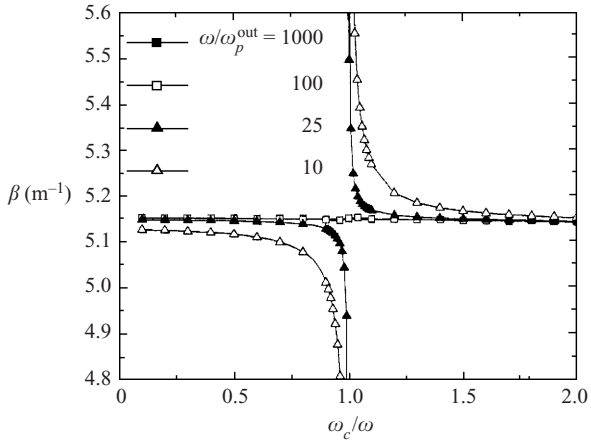

Figure 6. Axial wavenumber β as a function of ω/ω_c. The results were obtained for $\omega/\omega_p^{in} = 0.1$.

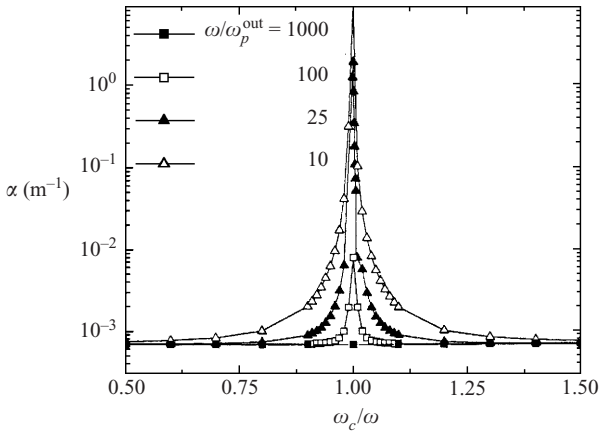

Figure 7. Axial attenuation coefficient α as a function of ω/ω_c values. The results were obtained for $\omega/\omega_p^{in} = 0.1$.

that the permittivity approaches that of free space. In addition, as the outer plasma density tends toward its critical value, it can be seen that $\beta \to 0$ when the ECR is appproached from the left side, while $\beta \to \infty$ when the ECR is approached from the right side. When considering the wave attenuation characteristics represented in Fig. 7, it can be seen that α shows a narrow peak at $\omega_c/\omega = 1$, the amplitude of this peak decreasing with the outer plasma density until no more peak is observed for $\omega/\omega_p^{out} = 1000$. From these results, we can reasonably believe that when the outer plasma density approaches its critical value, a cutoff occurs on the left side of $\omega_c/\omega = 1$ while a resonance occurs on the right side.

When examining Figs 6 and 7, it is clear that the width of the resonance is strongly influenced by the density of the outer plasma, thus suggesting that the resonance phenomenon occurs in the outer region. This results from the fact that in the outer medium, the dominant electric field component is radial. This fact is well known when the outer plasma is free space (Moisan et al. 1982), and we have

https://doi.org/10.1017/S0022377801001489 Published online by Cambridge University Press

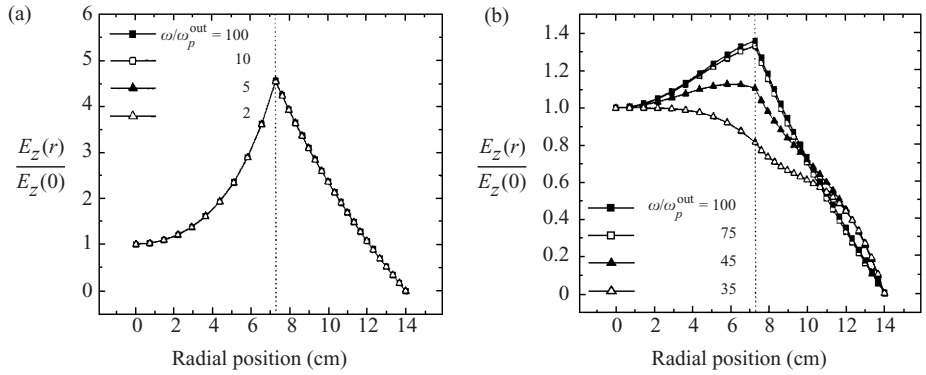

Figure 8. Radial intensity distribution of the axial component of the wave electric field for different values of ω/ω_p^{out} in (a) the unmagnetized case and (b) the magnetized ($\omega_c/\omega = 20$) plasma–plasma–metal case. The results have been obtained for $\omega/\omega_p^{in} = 0.1$ and normalized to 1 at $r = 0$. Note that in (a), all the curves corresponding to the different ω/ω_p^{out} are superimposed.

verified that this remains true when the outer region is filled with an underdense plasma. On the contrary, in the inner plasma, the dominant electric field component is axial, so that it cannot support any resonance.

3.2. Radial electromagnetic field distribution

When assuming a collisionless unmagnetized plasma–dielectric configuration (this includes the plasma–air case), the surface wave is purely evanescent in the transverse direction, i.e. in both the plasma and the dielectric layer (Margot and Moisan 1993). A consequence of this evanescence is that the electromagnetic field components are maximum at the plasma–dielectric interface. Figure 8(a) shows the radial profile of the axial component of the wave electric field for different outer plasma densities in the unmagnetized plasma–plasma–metal case. As can be seen, for all ω/ω_p^{out} values, the radial distribution exhibits a peak at the plasma–plasma interface, which means that the surface character of the wave is maintained. We further note that the distribution is not affected by the outer plasma density value in this case.

It was shown in Margot and Moisan (1991) that the radial distribution of the axial electric field $E_z(r)$ is considerably modified when an important magnetic field is applied to a plasma–dielectric system. For the $m = 0$ mode, the penetration depth increases with ω_c/ω. For the plasma–plasma–metal configuration, Fig. 8(b) shows the influence of the outer plasma density on the radial distribution of the axial electric field component when a strong magnetic field is applied, i.e. $\omega_c/\omega = 20$. It can be seen by comparison with Fig. 8(a) that, for a given $\omega/\omega_p^{out} = 100$, the penetration depth increases with the magnetic field intensity, since the value of $E_z(r)/E_z(0)$ at the plasma–plasma interface (i.e. $r = 7.3$ cm) decreases from 4.5 to 1.3 when ω_c/ω varies from 0 to 20. In contrast with the unmagnetized plasma–plasma–metal case shown in Fig. 8(a), Fig. 8(b) shows that the influence of the outer plasma density is significant when a strong enough magnetic field is applied. When ω/ω_p^{out} decreases, the wave even loses its surface character and the axial component of the electric field becomes maximum on the axis of the cylinder.

https://doi.org/10.1017/S0022377801001489 Published online by Cambridge University Press

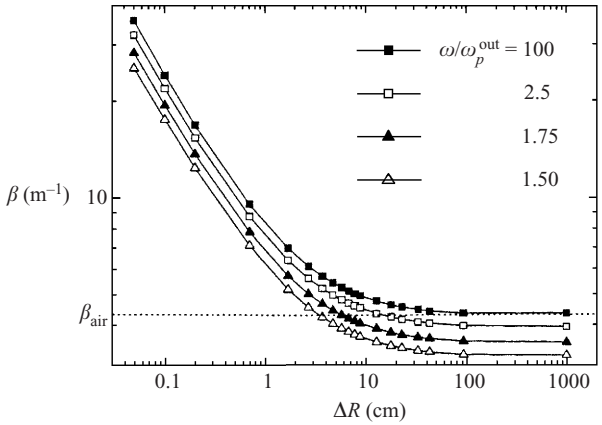

Figure 9. Influence of the outer plasma thickness ΔR on the axial wavenumber β in an unmagnetized plasma for $\omega/\omega_p^{in} = 0.1$.

3.3. Influence of the outer plasma dimension

We consider in this subsection the influence on the wave characteristics of the outer plasma thickness, defined as $\Delta R = b - a$. Note that for the plasma–plasma–metal configuration considered in this paper, the system can be seen as a waveguide filled with plasma surrounded by a sheath, when the outer plasma density is very small ($\omega/\omega_p^{out} \geqslant 100$) and ΔR becomes comparable to a few Debye lengths. For any value of ΔR, this situation corresponds to the case of a plasma–air metal configuration, in which the solution to the determinental equation $\mathrm{Det}\,\mathbf{T} = 0$ are known to be of two types (Boisse-Laporte 1993). The first type correponds to waveguide modes disturbed by the presence of the plasma, while the second corresponds to the surface-wave modes. In the following, we limit our investigation to the surface-wave solutions.

Figure 9 shows the variation of the wavenumber β as a function of the thickness ΔR for different values of the outer plasma density and for a constant inner plasma density. Note that the inner plasma radius is kept constant and equal to 7.3 cm. For large values of both ω/ω_p^{out} and ΔR, Fig. 9 shows that β tends toward a constant value. In this range of ΔR, the presence of the metal boundary can be neglected, so that the solution obtained corresponds to that of the plasma–air configuration (Margot and Moisan 1991), represented by the dashed line.

In addition, it can be seen that as ΔR decreases, the value of β in this case strongly increases. For example, as ΔR changes from 100 cm to 0.1 cm, β increases by about a factor of 10. This is expected, since, as shown by Trivelpiece (1967), surface waves do not exist for a traditionally homogeneous plasma surrounded by metal, so β must tends to ∞ when $\Delta R \to 0$. Finally, we have shown in Sec. 3.1 that β is decreasing with ω/ω_p^{out} below the ECR for $\Delta R = 6.7$ cm. Figure 9 shows that this remains true for any value of ΔR.

4. Conclusions

In this paper, we have examined the possibility of propagating azimuthally symmetric surface waves in plasma–plasma–metal structures in which the outer plasma is underdense. Outside the ECR conditions, the presence of the outer plasma plays

https://doi.org/10.1017/S0022377801001489 Published online by Cambridge University Press

a role similar to that of an ordinary dielectric layer, just modifying the wavenumber value without drastically changing its general characteristics. We have also shown that a resonance/cutoff behavior occurs on each side of the ECR as the outer plasma density tends toward its critical value. This feature, which disappears as the outer-plasma permittivity approaches that of free space, results from the fact that the electric field is essentially radial in the outer plasma layer. In addition, we have seen that the radial structure of the wave electromagnetic field is significantly affected by the outer plasma density only in the strongly magnetized case. Finally, the influence of the outer-plasma thickness was also investigated. The surface-wave solutions found for small outer-plasma thickness indicate that it is possible to propagate electromagnetic surface waves in waveguides filled with plasma, provided the latter is separated from the metal structure by at least a plasma sheath.

Finally, since the results presented in this paper were inspired by an existing experimental setup, the parameters used for calculations were intentionally chosen as realistic. However, it remains to confirm the calculations through appropriate experimental verification, which is not an obvious matter because of the complications related to phase and attenuation measurements within a plasma. On the other hand, the results obtained with the two-step density profile approximation considered in this paper are expected to differ slightly from those determined experimentally, because the density profile is actually continuous. It is, however, difficult to exactly predict the behavior of α and β under these circumstances, since for the $m = 0$ mode and in the absence of a magnetic field, the radial inhomogeneity of the plasma makes the attenuation coefficient and the wavenumber increase with the degree of inhomogeneity. In contrast, in the presence of a magnetic field of sufficient strength, α and β both decrease for an increasing degree of inhomogeneity. Nevertheless, the two-step density profile approximation used in the present paper should still provide a realistic estimation of the wave characteristics.

Acknowledgements

This work was supported by the Natural Science and Engineering Research Council of Canada (NSERC) and by the Network of Centres of Excellence in Microelectronics MICRONET.

References

Allis, W. P., Buschbaum, S. J. and Bers, A. 1963 *Waves in Anisotropic Plasmas*. Cambridge, MA: MIT Press.

Boisse-Laporte, C. 1993 Wave propagation in bounded plasmas. In: *Microwave Discharges Fundamental and Applications* (ed. C. M. Ferreira and M. Moisan). New York: Plenum, pp. 25–43.

Coopersberg, D. J. and Birdsall, C. K. 1998 Surface wave sustained plasmas in a metal bound plasma slab. *Plasma Sources Sci. Technol.* **7**, 41–53.

Delprat, S., Chaker M. and Margot, J. 1999 Patterned platinum etching studies in an argon high-density plasma. *Jpn J. Appl. Phys.* **38**, 4488–4491.

Ferreira, M. and Moisan, M. 1988 The similarity laws for the maintenance field and the absorbed power per electron in low-pressure surface-wave produced plasmas and their extension to HF plasmas in general. *Physica Scripta* **38**, 382.

Margot, J. and Moisan, M. 1991 Electromagnetic surface waves for a new approach to the investigation of plasmas produced at electron cyclotron resonance. *J. Phys. D: Appl. Phys.* **24**, 1765–1788.

Margot, J. and Moisan, M. 1993 Characteristics of surface wave propagation in dissipative cylindrical plasma columns. *J. Plasma Phys.* **49**, 357–374.

Margot, J. and Moisan, M. 1997 Physics of surface waves discharges. In: *Plasma Processing of Semiconductors* (ed. P. F. Williams). Dordrecht: Kluwer, pp. 187–210.

Moisan, M. and Zakrzewski, Z. 1991 Plasma sources based on the propagation of electromagnetic surface waves. *J. Phys. D: Appl. Phys.* **24**, 1025–1048.

Moisan, M., Shivarova, A. and Trivelpiece, A. W. 1982 Experimental investigation of the propagation of surface waves along a plasma column. *J. Plasma Phys.* **24**, 1331–1400.

Moisan, M., Hubert, J., Margot, J. and Zakrzewski, Z. 1999 The development and use of surface-wave discharges for applications. In: *Advanced Technologies Based on Wave and Beam Generated Plasmas* (ed. H. Schlüter and A. Shivarova). Dordrecht: Kluwer, pp. 23–64.

Morita, S., Nagatsu, M., Ghanashev, I., Toyoda, N. and Sugai, H. 1998 Production of low-pressure non-magnetized plasmas sustained under a dielectric-free metal–plasma interface. *Jpn J. Appl. Phys.* **37**, L468–L470.

Pasquiers, S., Boisse-Laporte, C., Granier, A., Bloyet, E., Leprince, P. and Marec, J. 1989 Action of a static magnetic field on an argon discharge produced by a travelling wave. *J. Appl. Phys.* **65**, 1765–1768.

St-Onge, L., Margot, J. and Chaker, M. 1998 Experimental investigation of a large SF_6 magnetoplasma source based on surface wave propagation. *Plasma Sources Sci. Technol.* **7**, 154–161.

Shkarofski, I. P. Johnston, T. W. and Bachynski M. P. 1966 *The Particle Kinetics of Plasmas.* Reading, MA: Addison-Wesley.

Sugai, H., Ghanashev, I. and Nagatsu, M. 1998 High-density flat plasma production based on surface waves. *Plasma Sources Sci. Technol.* **7**, 192–205.

Trivelpiece, A. W. 1967 *Slow Wave Propagation in Plasma Waveguides.* San Francisco Press.

Trivelpiece, A. W. and Gould, R. W. 1959 Space charge waves in cylindrical plasma columns. *J. Appl. Phys.* **30**, 1784–1793.

Zhelyazkov, I. and Atanassov, V. 1995 Axial structure of low-pressure high-frequency discharge by travelling electromagnetic surface waves. *Phys. Rep.* **255**, 82–201.